arXiv:1705.07028v3 [physics.ins-det] 12 Sep 2017

Prepared for submission to JINST

Cryogenic Characterization of FBK RGB-HD SiPMs

C. E. Aalseth,[a] F. Acerbi,[b,c] P. Agnes,[d] I. F. M. Albuquerque,[e] T. Alexander,[a] A. Alici,[f,g] A. K. Alton,[h] P. Ampudia,[i,j] P. Antonioli,[g] S. Arcelli,[f,g] R. Ardito,[k,l] I. J. Arnquist,[a] D. M. Asner,[a] H. O. Back,[a] G. Batignani,[m,n] E. Bertoldo,[o] S. Bettarini,[m,n] M. G. Bisogni,[m,n] V. Bocci,[p] A. Bondar,[q,r] G. Bonfini,[s] W. Bonivento,[j] M. Bossa,[t,s] B. Bottino,[u,v] R. Bunker,[a] S. Bussino,[x,y] A. Buzulutskov,[q,r] M. Cadeddu,[z,j] M. Cadoni,[z,j] A. Caminata,[v] N. Canci,[d,s] A. Candela,[s] C. Cantini,[ac] M. Caravati,[z,j] M. Cariello,[v] M. Carlini,[s] M. Carpinelli,[ae,af] A. Castellani,[k,l] S. Catalanotti,[aa,ab] V. Cataudella,[aa,ab] P. Cavalcante,[ag,s] R. Cereseto,[v] Y. Chen,[d] A. Chepurnov,[ah] A. Chiavassa,[ai,aj] C. Cicalò,[j] L. Cifarelli,[f,g] M. Citterio,[l] A. G. Cocco,[ab] M. Colocci,[f,g] S. Corgiolu,[i,j] G. Covone,[aa,ab] P. Crivelli,[ac] I. D'Antone,[g] M. D'Incecco,[s] M. D. Da Rocha Rolo,[aj] M. Daniel,[ak] S. Davini,[v,t] A. De Candia,[aa,ab] S. De Cecco,[al,p] M. De Deo,[s] G. De Filippis,[aa,ab] G. De Guido,[am,l] G. De Rosa,[aa,ab] G. Dellacasa,[aj] P. Demontis,[ae,af,an] A. V. Derbin,[ao] A. Devoto,[z,j] F. Di Eusanio,[ap] G. Di Pietro,[s,l] C. Dionisi,[al,p] A. Dolgov,[r] I. Dormia,[am,l] S. Dussoni,[m,n] A. Empl,[d] A. Ferri,[b,c] C. Filip,[aq] G. Fiorillo,[aa,ab] K. Fomenko,[ar] D. Franco,[as] G. E. Froudakis,[at] F. Gabriele,[s] A. Gabrieli,[ae,af] C. Galbiati,[ap,l] P. Garcia Abia,[ak] A. Gendotti,[ac] A. Ghisi,[k,l] S. Giagu,[al,p] G. Gibertoni,[am,l] C. Giganti,[au] M. Giorgi,[m,n] G. K. Giovanetti,[ap] M. L. Gligan,[aq] A. Gola,[b,c] O. Gorchakov,[ar] A. M. Goretti,[s] F. Granato,[av] M. Grassi,[m] J. W. Grate,[a] G. Y. Grigoriev,[ax] M. Gromov,[ah] M. Guan,[ay] M. B. B. Guerra,[az] M. Guerzoni,[g] M. Gulino,[ba,af] R. K. Haaland,[bb] B. Harrop,[ap] E. W. Hoppe,[a] S. Horikawa,[ac] B. Hosseini,[j] D. Hughes,[ap] P. Humble,[a] E. V. Hungerford,[d] An. Ianni,[ap,s] S. Jimenez Cabre,[ak] T. N. Johnson,[bc] K. Keeter,[az] C. L. Kendziora,[bd] S. Kim,[av] G. Koh,[ap] D. Korablev,[ar] G. Korga,[d,s] A. Kubankin,[be] R. Kugathasan,[aj,bt] M. Kuss,[m] X. Li,[ap] M. Lissia,[j] G. U. Lodi,[am,l] B. Loer,[a] G. Longo,[aa,ab] R. Lussana,[bf,l] L. Luzzi,[bg,l] Y. Ma,[ay] A. A. Machado,[bh] I. N. Machulin,[ax,bi] L. Mais,[i,j] A. Mandarano,[t,s,1] L. Mapelli,[ap] M. Marcante,[bj,c,b] A. Margotti,[g] S. M. Mari,[x,y] M. Mariani,[bg,l] J. Maricic,[bk] M. Marinelli,[u,v] D. Marras,[j] C. J. Martoff,[av] M. Mascia,[i,j] A. Messina,[al,p] P. D. Meyers,[ap] R. Milincic,[bk] A. Moggi,[m] S. Moioli,[am,l] S. Monasterio,[i,j] J. Monroe,[bs] A. Monte,[ad] M. Morrocchi,[m,n] W. Mu,[ac] V. N. Muratova,[ao] S. Murphy,[ac] P. Musico,[v] R. Nania,[g] J. Napolitano,[av] A. Navrer Agasson,[au] I. Nikulin,[be] V. Nosov,[q,r] A. O. Nozdrina,[ax,bi] N. N. Nurakhov,[ax] A. Oleinik,[be] V. Oleynikov,[q,r] M. Orsini,[s] F. Ortica,[bl,bm] L. Pagani,[u,v] M. Pallavicini,[u,v] S. Palmas,[i,j] L. Pandola,[af] E. Pantic,[bc] E. Paoloni,[m,n] G. Paternoster,[b,c] V. Pavletcov,[ah] F. Pazzona,[ae,af] K. Pelczar,[bn] L. A. Pellegrini,[am,l] N. Pelliccia,[bl,bm] F. Perotti,[k,l] R. Perruzza,[s] C. Piemonte,[b,c] F. Pilo,[m] A. Pocar,[ad] D. Portaluppi,[bo,l] S. S. Poudel,[d] D. A. Pugachev,[ax] H. Qian,[ap] B. Radics,[ac] F. Raffaelli,[m] F. Ragusa,[bp,l] K. Randle,[ap] M. Razeti,[j] A. Razeto,[s,ap,1] V. Regazzoni,[bj,c,b] C. Regenfus,[ac] B. Reinhold,[bk]

---

[1] Corresponding authors.

A. L. Renshaw,[d] **M. Rescigno,**[p] **Q. Riffard,**[as] **A. Rivetti,**[aj] **A. Romani,**[bl,bm] **L. Romero,**[ak]
B. Rossi,[ab] **N. Rossi,**[s] **A. Rubbia,**[ac] **D. Sablone,**[ap,s] **P. Salatino,**[bq,ab] **O. Samoylov,**[ar]
W. Sands,[ap] **M. Sant,**[ae,af] **R. Santorelli,**[ak] **C. Savarese,**[t,s] **E. Scapparone,**[g] **B. Schlitzer,**[bc]
G. Scioli,[f,g] **E. Sechi,**[i,j] **E. Segreto,**[bh] **A. Seifert,**[a] **D. A. Semenov,**[ao] **S. Serci,**[j] **A. Shchagin,**[be]
L. Shekhtman,[q,r] **E. Shemyakina,**[q,r] **A. Sheshukov,**[ar] **M. Simeone,**[bq,ab] **P. N. Singh,**[d]
M. D. Skorokhvatov,[ax,bi] **O. Smirnov,**[ar] **G. Sobrero,**[v] **A. Sokolov,**[q,r] **A. Sotnikov,**[ar]
C. Stanford,[ap] **G. B. Suffritti,**[ae,af,an] **Y. Suvorov,**[br,s,ax] **R. Tartaglia,**[s] **G. Testera,**[v]
A. Tonazzo,[as] **A. Tosi,**[bo,l] **P. Trinchese,**[aa,ab] **E. V. Unzhakov,**[ao] **A. Vacca,**[i,j] **M. Verducci,**[al,p]
T. Viant,[ac] **F. Villa,**[bo,l] **A. Vishneva,**[ar] **B. Vogelaar,**[ag] **M. Wada,**[ap] **J. Wahl,**[a] **S. Walker,**[aa,ab]
H. Wang,[br] **Y. Wang,**[ay,br] **A. W. Watson,**[av] **S. Westerdale,**[ap] **J. Wilhelmi,**[av] **R. Williams,**[a]
M. M. Wojcik,[bn] **S. Wu,**[ac] **X. Xiang,**[ap] **X. Xiao,**[br] **C. Yang,**[ay] **Z. Ye,**[d] **F. Zappa,**[bo,l]
G. Zappalà,[bj,c,b] **C. Zhu,**[ap] **A. Zichichi,**[f,g] **G. Zuzel**[bn]

[a] *Pacific Northwest National Laboratory, Richland, WA 99352, USA*
[b] *Fondazione Bruno Kessler, Povo 38123, Italy*
[c] *Trento Institute for Fundamental Physics and Applications, Povo 38123, Italy*
[d] *Department of Physics, University of Houston, Houston, TX 77204, USA*
[e] *Instituto de Física, Universidade de São Paulo, São Paulo 05508-090, Brazil*
[f] *Physics Department, Università degli Studi di Bologna, Bologna 40126, Italy*
[g] *INFN Bologna, Bologna 40126, Italy*
[h] *Physics Department, Augustana University, Sioux Falls, SD 57197, USA*
[i] *Department of Mechanical, Chemical, and Materials Engineering, Università degli Studi, Cagliari 09042, Italy*
[j] *INFN Cagliari, Cagliari 09042, Italy*
[k] *Civil and Environmental Engineering Department, Politecnico di Milano, Milano 20133, Italy*
[l] *INFN Milano, Milano 20133, Italy*
[m] *INFN Pisa, Pisa 56127, Italy*
[n] *Physics Department, Università degli Studi di Pisa, Pisa 56127, Italy*
[o] *INFN Milano Bicocca, Milano 20126, Italy*
[p] *INFN Sezione di Roma, Roma 00185, Italy*
[q] *Budker Institute of Nuclear Physics, Novosibirsk 630090, Russia*
[r] *Novosibirsk State University, Novosibirsk 630090, Russia*
[s] *INFN Laboratori Nazionali del Gran Sasso, Assergi (AQ) 67100, Italy*
[t] *Gran Sasso Science Institute, L'Aquila 67100, Italy*
[u] *Physics Department, Università degli Studi di Genova, Genova 16146, Italy*
[v] *INFN Genova, Genova 16146, Italy*
[x] *INFN Roma Tre, Roma 00146, Italy*
[y] *Mathematics and Physics Department, Università degli Studi Roma Tre, Roma 00146, Italy*
[z] *Physics Department, Università degli Studi di Cagliari, Cagliari 09042, Italy*
[aa] *Physics Department, Università degli Studi "Federico II" di Napoli, Napoli 80126, Italy*
[ab] *INFN Napoli, Napoli 80126, Italy*
[ac] *Institute for Particle Physics, ETH Zürich, Zürich 8093, Switzerland*
[ad] *Amherst Center for Fundamental Interactions and Physics Department, University of Massachusetts, Amherst, MA 01003, USA*

[ae] Chemistry and Pharmacy Department, Università degli Studi di Sassari, Sassari 07100, Italy
[af] INFN Laboratori Nazionali del Sud, Catania 95123, Italy
[ag] Virginia Tech, Blacksburg, VA 24061, USA
[ah] Skobeltsyn Institute of Nuclear Physics, Lomonosov Moscow State University, Moscow 119991, Russia
[ai] Physics Department, Università degli Studi di Torino, Torino 10125, Italy
[aj] INFN Torino, Torino 10125, Italy
[ak] CIEMAT, Centro de Investigaciones Energéticas, Medioambientales y Tecnológicas, Madrid 28040, Spain
[al] Physics Department, Sapienza Università di Roma, Roma 00185, Italy
[am] Chemistry, Materials and Chemical Engineering Department "G. Natta", Politecnico di Milano, Milano 20133, Italy
[an] Interuniversity Consortium for Science and Technology of Materials, Firenze 50121, Italy
[ao] Saint Petersburg Nuclear Physics Institute, Gatchina 188350, Russia
[ap] Physics Department, Princeton University, Princeton, NJ 08544, USA
[aq] National Institute for R&D of Isotopic and Molecular Technologies, Cluj-Napoca, 400293, Romania
[ar] Joint Institute for Nuclear Research, Dubna 141980, Russia
[as] APC, Université Paris Diderot, CNRS/IN2P3, CEA/Irfu, Obs de Paris, USPC, Paris 75205, France
[at] Department of Chemistry, University of Crete, P.O. Box 2208, 71003 Heraklion, Crete, Greece
[au] LPNHE, Université Pierre et Marie Curie, CNRS/IN2P3, Sorbonne Universités, Paris 75252, France
[av] Physics Department, Temple University, Philadelphia, PA 19122, USA
[ax] National Research Centre Kurchatov Institute, Moscow 123182, Russia
[ay] Institute of High Energy Physics, Beijing 100049, China
[az] School of Natural Sciences, Black Hills State University, Spearfish, SD 57799, USA
[ba] Civil and Environmental Engineering Department, Università degli Studi di Enna "Kore", Enna 94100, Italy
[bb] Department of Physics and Engineering, Fort Lewis College, Durango, CO 81301, USA
[bc] Department of Physics, University of California, Davis, CA 95616, USA
[bd] Fermi National Accelerator Laboratory, Batavia, IL 60510, USA
[be] Radiation Physics Laboratory, Belgorod National Research University, Belgorod 308007, Russia
[bf] Electronics, Information, and Bioengineering Department, Politecnico di Milano, Milano 20133, Italy
[bg] Energy Department, Politecnico di Milano, Milano 20133, Italy
[bh] Physics Institute, Universidade Estadual de Campinas, Campinas 13083, Brazil
[bi] National Research Nuclear University MEPhI, Moscow 115409, Russia
[bj] Physics Department, Università degli Studi di Trento, Povo 38123, Italy
[bk] Department of Physics and Astronomy, University of Hawai'i, Honolulu, HI 96822, USA
[bl] Chemistry, Biology and Biotechnology Department, Università degli Studi di Perugia, Perugia 06123, Italy
[bm] INFN Perugia, Perugia 06123, Italy
[bn] M. Smoluchowski Institute of Physics, Jagiellonian University, 30-348 Krakow , Poland
[bo] Electronics, Information, and Bioengineering Department, Politecnico di Milano, Milano 20133, Italy
[bp] Physics Department, Università degli Studi di Milano, Milano 20133, Italy
[bq] Chemical, Materials, and Industrial Production Engineering Department, Università degli Studi "Federico II" di Napoli, Napoli 80126, Italy
[br] Physics and Astronomy Department, University of California, Los Angeles, CA 90095, USA
[bs] Department of Physics, Royal Holloway University of London, Egham TW20 0EX, UK
[bt] Department of Electronics and Communications, Politecnico di Torino, Torino 10129, Italy

E-mail: `sarlabb@lngs.infn.it`

Abstract: We report on the cryogenic characterization of Red Green Blue - High Density (RGB-HD) SiPMs developed at Fondazione Bruno Kessler (FBK) as part of the DarkSide program of dark matter searches with liquid argon time projection chambers. A cryogenic setup was used to operate the SiPMs at varying temperatures and a custom data acquisition system and analysis software were used to precisely characterize the primary dark noise, the correlated noise, and the gain of the devices. We demonstrate that FBK RGB-HD SiPMs with low quenching resistance (RGB-HD-LR$_q$) can be operated from 40 K to 300 K with gains in the range 10^5 to 10^6 and noise rates at a level of around 1 Hz/mm^2.

Keywords: SiPMs

Contents

1 Introduction **1**

2 RGB-HD SiPMs **1**

3 Setup and analysis **2**

4 Results **3**

5 Conclusions **6**

6 Acknowledgements **6**

1 Introduction

Silicon photomultipliers (SiPMs) are of special interest for the development of argon- and xenon-based cryogenic dark matter detectors, whose performance strongly depends on efficient detection of single scintillation photons. Operating SiPMs at cryogenic temperature (87 K for argon and 165 K for xenon) introduces both challenges and advantages over room temperature operation.

Building on its strong history of SiPM development [1–3], FBK [1] has developed a new generation of devices, the Red Green Blue - High Density (RGB-HD) SiPM [4]. We evaluated RGB-HD SiPMs for possible use as photosensors in the DarkSide program of liquid argon time projection chamber dark matter searches [5, 6]. Among the features required for use in the DarkSide program of experiments are a low dark rate ($< 100\,\mathrm{mHz/mm^2}$) and a total correlated noise probability lower than 60%. Both are necessary to maintain the detector energy resolution and pulse shape discrimination performance.

Cryogenic studies of SiPMs are already present in literature [7, 8]. This paper details the first study of the performance of FBK RGB-HD SiPMs in the temperature range from 40 K to 300 K. Section 2 introduces the two variants of RGB-HD SiPMs that we tested; section 3 gives a brief overview of the cryogenic setup, the readout chain, and the analysis software (for a more detailed description, we refer the reader to Ref. [9]); finally, in section 4, we detail the results obtained with these devices.

2 RGB-HD SiPMs

An introduction to the performance of RGB-HD SiPMs can be found in [4]. Here we focus on the cryogenic performance of RGB-HD SiPMs. We studied two variants of RGB-HD SiPMs, the RGB-HD High quenching Resistor (RGB-HD-HR$_q$) and the RGB-HD Low quenching Resistor

---

[1] Fondazione Bruno Kessler, Trento, Italy

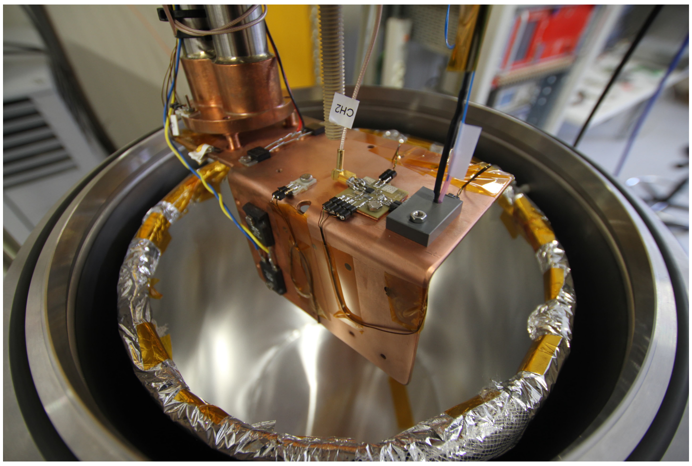

Figure 1. Detail of the cold finger, positioned just above the top opening of the stainless steel cylindrical cryostat. Also visible is the PTFE tube covered with superinsulator. On the right hand side of the cold finger, a black box contains the SiPM under test. Two unjacketed optical fibers, connected to an LED and to a laser source placed outside the vacuum chamber, penetrate the top side of the black box and can be used to deliver calibrated light signals to the SiPM under test. In the center of the cold finger is a cryogenic pre-amplifier and on the left are the cold head of the cryocooler and the set of high power film resistors used to control the temperature.

(RGB-HD-LR$_q$). The RGB-HD-HR$_q$ SiPMs reported here were fabricated with a SPAD size of $25 \times 25\,\mu\mathrm{m}^2$ and the RGB-HD-LR$_q$ SiPMs had a SPAD size of $20 \times 20\,\mu\mathrm{m}^2$. The capacitance per unit area is $50\,\mathrm{pF/mm}^2$ in both cases. All the SiPMs tested were $5 \times 5\,\mathrm{mm}^2$.

3 Setup and analysis

The cryogenic setup is contained in a stainless steel cryostat sealed with two DN 320 ISO-K flanges and pumped to a vacuum level of about 10^{-2} mbar with a Pfeiffer ACP15 multi-stage roots evacuation pump. A Cryomech PT90 pulse tube cryocooler, with 90 W of cooling capacity at 77 K, is mounted to the top flange of the cryostat. The cold head of the cryocooler is equipped with a cold finger that holds the SiPM assembly under test, as shown in Figure 1. The system is optimized for fast thermal cycling: the cold finger can be cooled down to 40 K in about 40 min. The cold finger is also equipped with a platinum RTD connected to a Lakeshore 335 temperature controller that supplies a set of high power metal film resistors mounted on the cold finger with the thermal load required for temperature regulation. The top flange also hosts feedthroughs for two optical fibers that are connected to an external LED and a laser light source. They can be used for measurements of the photon detection efficiency (PDE) of SiPMs, although this is not within the scope of this work and will be subject of a future study.

The readout chain is composed of a Keithley 2450 SourceMeter that serves as the bias source for the SiPM; a cryogenic pre-amplifier, based on a high speed, low-noise operational amplifier configured as a trans-impedance amplifier (TIA) with a feedback resistor of $500\,\Omega$, resulting in a gain of $0.5\,\mathrm{mV}/\mu\mathrm{A}$; a single stage, non-inverting warm amplifier, configured for a gain of $28.8\,\mathrm{V/V}$; and a CAEN V1751 1 GS/s 10 bit digitizer configured for interleaved acquisition and operating in auto-trigger mode. The TIA was characterized over the full range of test temperatures to verify that it made no temperature dependent contribution to the SiPM performance [10].

A custom data analysis software developed at FBK reads the data saved by the digitizer and performs a detailed analysis of the SiPM response. For each event, the program calculates the peak amplitude and the time since the previous event and then generates a scatter plot of these two parameters. An example of a scatter plot from an RGB-HD-HR$_q$ operated at 40 K and 4 V over-voltage is shown in Fig. 2. From this figure it is possible to identify the noise sources that compose the response of the device:

- DCR: the main group of events is primary dark count rate (DCR), with an amplitude centered around 1 PE (Photo-Electron) and an exponential time distribution;
- DiCT: Direct CrossTalk (DiCT) events occur when, after a primary event, a photon triggers a second avalanche in a neighboring cell. Since the travel time is of the order of picoseconds, it is impossible to resolve the two events. As a result, DiCT events have a time distribution similar to that of DCR but a greater amplitude (2 or more PE);
- DeCT: Delayed CrossTalk (DeCT) is characterized by delay times of the order of a few to tens of nanoseconds. Such events occur when crosstalk photons are absorbed in the non-depleted region of a neighboring cell. The carriers then have to diffuse into the high-field region before triggering an avalanche. The resulting pulses have an amplitude of 1 PE but are delayed with respect to the previous ones by the characteristic diffusion time;
- AP: AfterPulsing events have intermediate delay times and an amplitude of 1 PE or lower. Such events occur when an electron produced in an avalanche is trapped by some impurity in the silicon lattice and is then released after a characteristic time, producing a second avalanche in the same cell. The time distribution is therefore correlated to the trap time constant and the recharge time constant of the microcell. If the time distance is lower than the latter, the AP event will have a reduced amplitude.

The breakdown voltage at each test temperature is calculated by analyzing the waveform amplitude using the DLED algorithm [11], this is done automatically by the software. The peak amplitude has a linear dependence on the applied over-voltage and allows a precise determination of V_{bd} (see Fig. 3). This value is then used to correct the bias voltage so that the SiPMs are tested at the same over-voltages at each temperature.

4 Results

As discussed in Ref. [9], all FBK SiPMs are passively quenched using a polysilicon resistor. This resistance increases as temperature decreases, which leads to an increase in the single cell recharge time and hence the slow component of the SiPM pulse, τ_s. Operation at cryogenic temperature therefore increases the length of the SiPM signal to several microseconds, leading to incomplete integration of the released charge within a 500 ns gate. RGB-HD-LR$_q$ SiPMs were developed with a low resistance that depends weakly on temperature to overcome this problem. This reduces the temperature variation of the SPAD recharge time so that even at the 87 K argon boiling point, the

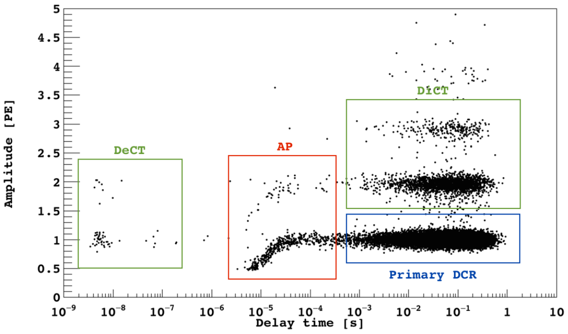

Figure 2. Distribution of peak amplitude versus time since last event for an RGB-HD-HR$_q$ SiPM operating at 40 K and 4 V of over-voltage in the absence of light. It is possible to identify the different noise components of the SiPM response described in the text: DCR, DiCT, DeCT and AP.

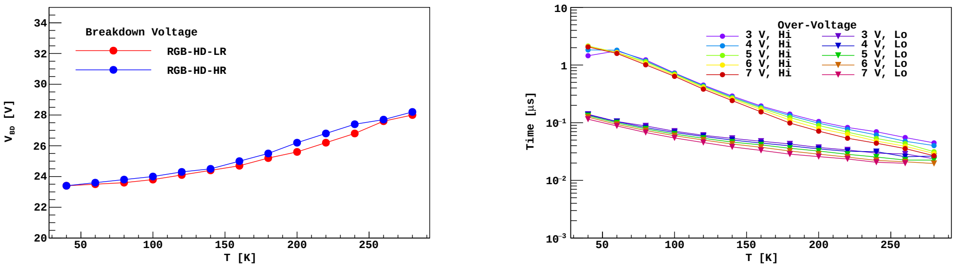

Figure 3. **Left:** Breakdown voltage for RGB-HD-HR$_q$ (blue markers) and RGB-HD-LR$_q$ (red markers) as a function of temperature. **Right:** SPAD recharge time constant as a function of over-voltage and temperature for the RGB-HD-HR$_q$ (circular markers) and RGB-HD-LR$_q$ (triangular markers) SiPMs.

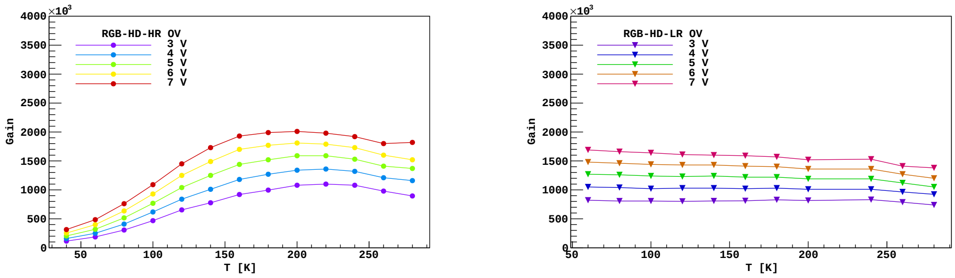

Figure 4. Gain as a function of over-voltage and temperature for the RGB-HD-HR$_q$ (left) and RGB-HD-LR$_q$ (right) SiPMs measured within a 500 ns integration gate.

SiPM signal is fully contained within 500 ns. Figure 3 shows the SPAD recharge time for both the RGB-HD-HR$_q$ and RGB-HD-LR$_q$ SiPMs. At low temperatures, the RGB-HD-LR$_q$ SiPMs have a recharge time one order of magnitude faster. The effect of the pulse length variation on the charge collected within the 500 ns gate is shown in Figure 4. The performance of the RGB-HD-LR$_q$ SiPM shows almost no variation, in contrast to the RGB-HD-HR$_q$ device. The fast peak of the pulse is

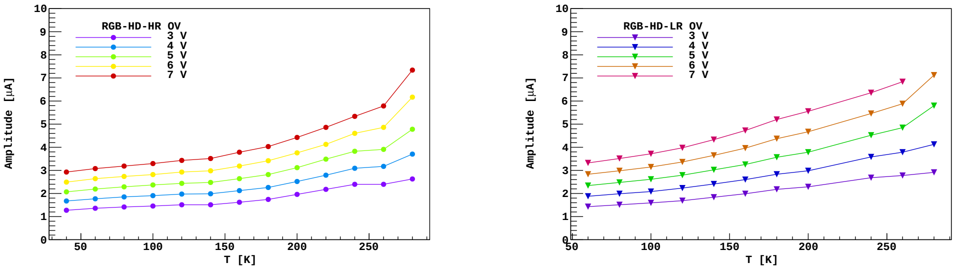

Figure 5. Amplitude of the average SPAD response as a function of over-voltage and temperature for the RGB-HD-HR$_q$ (left) and RGB-HD-LR$_q$ (right) SiPMs.

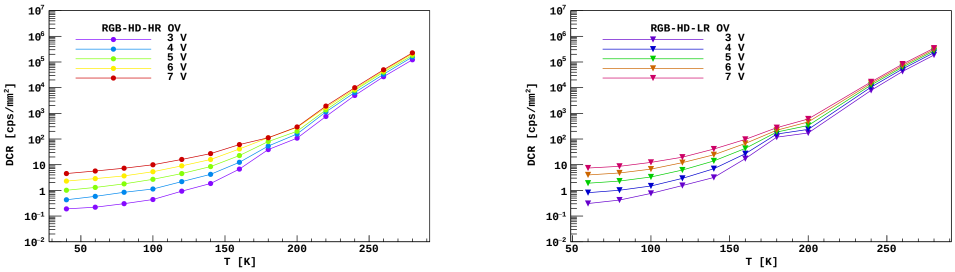

Figure 6. DCR as a function of over-voltage and temperature for the RGB-HD-HR$_q$ (left) and RGB-HD-LR$_q$ (right) SiPMs.

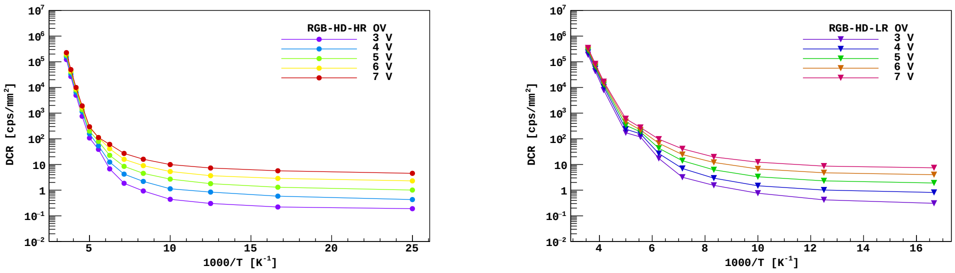

Figure 7. DCR as a function of over-voltage and the inverse of temperature for the RGB-HD-HR$_q$ (left) and RGB-HD-LR$_q$ (right) SiPMs. This representation allows the two mechanisms responsible for DCR to be distinguished: thermal generation (steep region) and field enhanced effects (plateau region).

almost unaffected by temperature. Its amplitude increases linearly with over-voltage and only very slowly with temperature for both devices, as shown in Figure 5.

The DCR as a function of temperature and over-voltage is shown in Fig. 6. When operated at low temperature, both variants show a DCR reduced by over five orders of magnitude relative to room temperature. The DCR for the two variants is of the same order of magnitude over the studied temperature range. The Arrhenius plot, shown in Figure 7, allows one to distinguish between the different mechanisms that give rise to the primary dark count rate. At high temperature (steep region), the dominant mechanism is thermal generation, which has an exponential dependence on temperature, while field-enhanced effects [12] dominate at low temperature, where the DCR reaches a plateau.

The two variants of RGB-HD technology have similar correlated noise levels. Direct cross

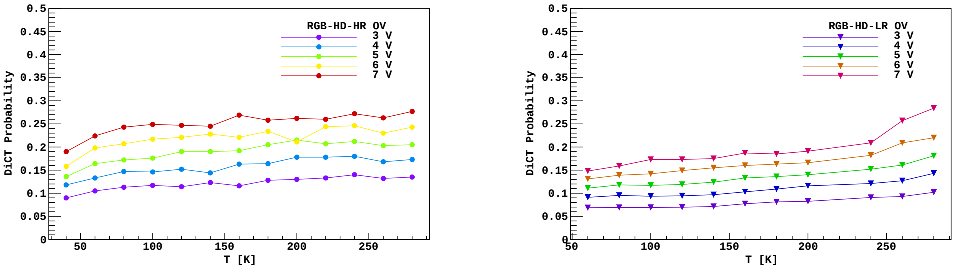

Figure 8. DiCT as a function of over-voltage and temperature for the RGB-HD-HR$_q$ (left) and RGB-HD-LR$_q$ (right) SiPMs.

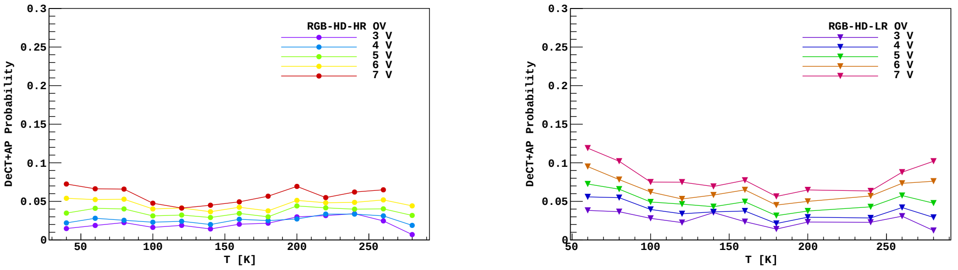

Figure 9. Sum of AP and DeCT as a function of over-voltage and temperature for the RGB-HD-HR$_q$ (left) and RGB-HD-LR$_q$ (right) SiPMs.

talk, shown in Figure 8, has a weak dependence on the temperature and increases linearly with over-voltage. Overall, the direct cross talk probability is lower for RGB-HD-LR$_q$ devices. DeCT and AP events partially overlap in time, especially at high temperatures, making it difficult to distinguish between the two. It is therefore more convenient to measure their sum, as shown in Fig. 9. For both SiPM variants, the sum of the DeCT and AP is less than 10 %.

5 Conclusions

We compared the performance of two variants of RGB-HD SiPMs produced by FBK in the temperature range from 40 K to 300 K. The RGB-HD-LR$_q$ SiPMs were shown to have a fast signal at low temperature that is fully contained within a 500 ns integration gate, gains in the range 10^5 to 10^6, noise rates around 1 Hz/mm^2 in the temperature range from 40 K to 300 K and total correlated noise probabilities below 50 %, satisfying the requirements for DarkSide-20k. These features make the RGB-HD-LR$_q$ SiPMs attractive for use in the DarkSide family of experiments.

6 Acknowledgements

The development of the NUV-HD and NUV-HD-LF SiPM technologies was funded by the EU FP7 project SUBLIMA, Grant 241711. We acknowledge support from NSF (US, Grant PHY-1314507 for Princeton University), the Istituto Nazionale di Fisica Nucleare (Italy) and Laboratori Nazionali del Gran Sasso (Italy).

References

[1] C. Piemonte, *A new Silicon Photomultiplier structure for blue light detection*, Nucl. Inst. Meth. A **568** (2006) 224–232.

[2] N. Dinu, R. Battiston, M. Boscardin, G. Collazuol, F. Corsi, G. F. Dalla Betta et al., *Development of the first prototypes of Silicon PhotoMultiplier (SiPM) at ITC-irst*, Nucl. Inst. Meth. A **572** (2007) 422–426.

[3] C. Piemonte, R. Battiston, M. Boscardin, G. F. Dalla Betta, A. Del Guerra, N. Dinu et al., *Characterization of the First Prototypes of Silicon Photomultiplier Fabricated at ITC-irst*, IEEE Trans. Nucl. Sci. **54** (2007) 236–244.

[4] A. Ferri, F. Acerbi, P. Fischer, A. Gola, G. Paternoster, C. Piemonte et al., *First results with SiPM tiles for TOF PET based on FBK RGB-HD technology*, EJNMMI Phys. **2** (2015) A86.

[5] P. Agnes, T. Alexander, A. K. Alton, K. Arisaka, H. O. Back, B. Baldin et al., *First results from the DarkSide-50 dark matter experiment at Laboratori Nazionali del Gran Sasso*, Phys. Lett. B **743** (2015) 456–466.

[6] P. Agnes, L. Agostino, I. F. M. Albuquerque, T. Alexander, A. K. Alton, K. Arisaka et al., *Results from the first use of low radioactivity argon in a dark matter search*, Phys. Rev. D **93** (2016) 081101.

[7] P. K. Lightfoot, G. J. Barker, K. Mavrokoridis, Y. A. Ramachers and N. J. C. Spooner, *Characterisation of a silicon photomultiplier device for applications in liquid argon based neutrino physics and dark matter searches*, *Journal of Instrumentation* **3** (2008) P10001.

[8] G. Collazuol, M. Bisogni, S. Marcatili, C. Piemonte and A. D. Guerra, *Studies of silicon photomultipliers at cryogenic temperatures*, *Nuclear Instruments and Methods in Physics Research Section A: Accelerators, Spectrometers, Detectors and Associated Equipment* **628** (2011) 389 – 392.

[9] F. Acerbi, S. Davini, A. Ferri, C. Galbiati, G. Giovanetti, A. Gola et al., *Cryogenic Characterization of FBK HD Near-UV Sensitive SiPMs*, IEEE Trans. Elec. Dev. (2017) 1–6.

[10] M. D'Incecco, C. Galbiati, G. K. Giovanetti, G. Korga, X. Li, A. Mandarano et al., *Development of a very low-noise cryogenic pre-amplifier for large-area SiPM devices*, `1706.04213`.

[11] A. Gola, C. Piemonte and A. Tarolli, *The DLED Algorithm for Timing Measurements on Large Area SiPMs Coupled to Scintillators*, IEEE Trans. Nucl. Sci. **59** (2012) 358–365.

[12] M. Ghioni, A. Gulinatti, I. Rech, P. Maccagnani and S. Cova, *Large-area low-jitter silicon single photon avalanche diodes*, Proc. SPIE **6900** (2008) 69001D–69001D–13.